Korea-Australia Rheology Journal
Vol. 14, No. 4, December 2002 pp. 161-174

Computation of viscoelastic flow using neural networks and stochastic simulation

D. Tran-Canh and T. Tran-Cong*
Faculty of Engineering and Surveying, University of Southern Queensland
Toowoomba, QLD 4350, Australia

(Received January 29, 2002; final revision received June 14, 2002)

Abstract

A new technique for numerical calculation of viscoelastic flow based on the combination of Neural Networks (NN) and Brownian Dynamics simulation or Stochastic Simulation Technique (SST) is presented in this paper. This method uses a "universal approximator" based on neural network methodology in combination with the kinetic theory of polymeric liquid in which the stress is computed from the molecular configuration rather than from closed form constitutive equations. Thus the new method obviates not only the need for a rheological constitutive equation to describe the fluid (as in the original Calculation Of Non-Newtonian Flows: Finite Elements & Stochastic Simulation Techniques (CONNFFESSIT) idea) but also any kind of finite element-type discretisation of the domain and its boundary for numerical solution of the governing PDE's. As an illustration of the method, the time development of the planar Couette flow is studied for two molecular kinetic models with finite extensibility, namely the Finitely Extensible Nonlinear Elastic (FENE) and FENE-Peterlin (FENE-P) models.

Keywords : Brownian dynamics, neural networks, molecular models, stochastic simulation, viscoelastic flow, diffusion equation, Fokker-Plank equation, Brownian simulation, CONNFFESSIT

1. Introduction

The computation of viscoelastic fluid flow has undergone strong development for the last three decades or so. Most common methods of numerical computation and analysis are macroscopic in nature where the system of mass and momentum conservation equations are supplemented by an appropriate closed form constitutive equation. The disadvantage appears for those models that cannot be cast into closed form (Hulsen *et al.*, 1997; Ottinger, 1996). Recently, a new technique, namely the CONNFFESSIT proposed by Laso and Ottinger (1993), has been introduced to bypass the need of a closed form constitutive equation. It is the combination between the traditional element method and the SST. The main idea of the CONNFFESSIT approach is that the polymer contribution to the stress is calculated from the configuration of a large ensemble of microscopic entities which acts as a stress calculator instead of a closed form constitutive equation (Ottinger, 1996; Laso and Ottinger, 1993; Feigl *et al.*, 1995; Laso *et al.*, 1997, 1999). This approach is an attempt to emulate the situation in real liquids, where the full information about the stress is contained in the configuration of molecules which results from the deformation history. However, the Finite Element Method (FEM) in CONNFFESSIT requires the discretisation of the domain under consideration into a number of finite elements (FE) which are defined by certain fixed topology in terms of a number of nodes. Breaking the original domain of analysis into a set of finite elements is not easy, specially for problems with moving boundaries, complex boundary or free surface.

In addition to the popular methods for the numerical solution of PDE's such as FEM, Boundary Element Method (BEM) and Finite Volume Method (FVM), more recent NN-based methods such as Radial Basis Function Networks (RNFNs) (Kansa, 1990; Zerroukat *et al.*, 1998; Mai-Duy and Tran-Cong, 2001), MultiLayer Perceptron Networks (MPLNs) (He *et al.*, 2000), Approximate Identity Networks (AINs) (Conti and Turchetti, 1994) prove to be promising. Such a NN-based method will be developed in the present work. Thus in contrast to FE-type approximations, the presently proposed Computation of Viscoelastic Flow by NN and SS method (CVFNNSS) is based on a direct combination of the stochastic simulation of molecular model of polymers with NN-based numerical techniques. In the present CVFNNSS method, the polymer stress is computed by a Brownian simulation technique as a component of the macromolecular approach (Hulsen *et al.*, 1997; Ottinger, 1996; Bird *et al.*, 1987; Fixman, 1978a, 1978b). The polymer-contributed stress is then used as position-dependent known

*Corresponding author: trancong@usq.edu.au

terms in solving the continuity and momentum equations in a macroscopic approach. The present method does not require any fixed connectivity to satisfy a predetermined topology, i.e. a mesh in which the elements are constrained by some geometrical regularity conditions (e.g. a positive volume). The present discrete model is completely represented by a set of unstructured discrete collocation nodes in the analysis domain and on its boundary in both microscopic and macroscopic part of the CVFNNSS procedure and therefore is referred to as a mesh-free numerical technique according to commonly cited concepts (Onate *et al.*, 1996; Belytschko *et al.*, 1996). The paper is organized as follows. In sections 2, 3, 4, the basic ideas of CVFNNSS are presented in which the governing equations and the stochastic simulation technique for computing the stress are described. In section 5, the NN-based numerical method for approximation of a function and its derivatives is presented briefly and the RBFN method for solving the conservation equations is described. Section 6 presents the algorithm of the CVFNNSS procedure, highlighting the macroscopic-microscopic interfaces of the method. The numerical examples are then discussed in section 7 with a brief conclusion in section 8.

2. Governing equations

Considering the isothermal flow of an incompressible fluid with density ρ, the system of momentum and mass conservation equations is given by

$$\rho\frac{\partial \boldsymbol{u}}{\partial t}+\rho(\boldsymbol{u}\cdot\nabla)\boldsymbol{u}=-\nabla p+\nabla\cdot\boldsymbol{\tau}, \tag{1}$$

$$\nabla\cdot\boldsymbol{u}=0 \tag{2}$$

where p is the pressure arisen from the incompressibility constraint; $\boldsymbol{u}$ denotes velocity field; $\boldsymbol{\tau}$ is the extra stress. The extra stress is then further decomposed as

$$\boldsymbol{\tau}=\boldsymbol{\tau}^{s}+\boldsymbol{\tau}^{p}, \tag{3}$$

where $\boldsymbol{\tau}^{s}=2\eta_{s}\boldsymbol{L}$ is the Newtonian solvent contribution; η_{s} is the solvent viscosity; $\boldsymbol{L}$ is the rate of strain tensor; $\boldsymbol{\tau}^{p}$ is the polymer-contributed stress. Using Eq. (3), Eq. (1) can be rewritten as follows

$$\rho\frac{\partial \boldsymbol{u}}{\partial t}+\rho(\boldsymbol{u}\cdot\nabla)\boldsymbol{u}=-\nabla p+\nabla\cdot(2\eta_{s}\boldsymbol{L}+\boldsymbol{\tau}^{p}) \tag{4}$$

In the traditional macroscopic approach the system is usually closed by the specification of a closed form constitutive equation for the polymer-contributed stress $\boldsymbol{\tau}^{p}$. In contrast, $\boldsymbol{\tau}^{p}$ is here calculated numerically via a microscopic technique. The overall macro-microscopic procedure is described in the next section.

3. The macro-microscopic approach

The general procedure for this approach is as follows. At each time step the polymer-contributed stress is assumed known from the previous iteration and the system of mass and momentum conservation equations is solved by a macroscopic numerical method. The velocity field thus obtained is then used in a stochastic simulation technique to calculate the polymer-contributed stress. The iteration is continued until convergence is achieved before advancing to the next time level.

The microscopic method employs the Brownian dynamics simulation to determine the stress via kinetic modelling (Ottinger, 1996; Bird *et al.*, 1987) which is described in the next section, followed by the description of a mesh-free collocation method for the solution of the continuity and momentum equations. All function approximations are based on the radial basis function networks and the overall procedure is free of finite-element-type discretisation and thus referred to as mesh-free.

In the next section, the stochastic simulation technique is presented for the computation of the polymer-contributed stress $\boldsymbol{\tau}^{p}$.

4. Stochastic simulation technique in polymeric kinetic theory

In polymer kinetic theory, the determination of polymer stresses is carried out through two steps (Ottinger, 1996; Laso and Ottinger, 1993; Feigl *et al.*, 1995; Laso *et al.*, 1997). The first step is to derive the diffusion equation or Fokker-Planck Equation for the configurational distribution function $\psi(\boldsymbol{Q},t)$ which is the probability density of the polymer configuration $\boldsymbol{Q}$ occurring at time t. The second step is to develop an expression for the stress tensor corresponding to the polymer configuration of which the distribution is expressed by $\psi(\boldsymbol{Q},t)$. The stochastic simulation is based on the relationship between the diffusion equation and the stochastic differential equation (SDE). The detail about the relationship between the diffusion equation and SDE is presented, for example, in Ottinger (1996); Laso and Ottinger (1993); Feigl *et al.* (1995); Laso *et al.* (1997) and Laso *et al.* (1999).

In this work, two non-linear dumbbell models, the FENE and FENE-P models, are studied using stochastic simulation technique. The FENE-P has a corresponding approximate closed form constitutive equation (Bird *et al.*, 1987) while the FENE model has not. These two dumbbell models are shown in Fig. 1 where the polymer configuration is described by the connector vector $\boldsymbol{Q}(t)$. The dynamics of polymeric liquids can be represented by the diffusion equation for $\psi(\boldsymbol{Q},t)$ and, in the absence of external forces, is given by (Ottinger, 1996; Feigl *et al.*, 1995; Bird *et al.*, 1987)

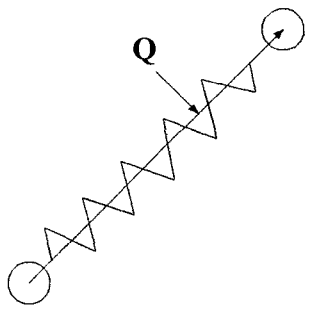

Fig. 1. Elastic dumbbell model: the connector vector Q describes the configuration of the model.

$$\rho\frac{\partial}{\partial t}\psi(\boldsymbol{Q},t)=\frac{\partial}{\partial \boldsymbol{Q}}\cdot[\boldsymbol{A}(\boldsymbol{Q},t)\psi(\boldsymbol{Q},t)] +\frac{1}{2}\frac{\partial}{\partial \boldsymbol{Q}}\cdot\left[\frac{\partial}{\partial \boldsymbol{Q}}\cdot\{\boldsymbol{D}(\boldsymbol{Q},t)\psi(\boldsymbol{Q},t)\}\right] \quad (5)$$

where $\boldsymbol{A}(\boldsymbol{Q},t)$ is a 3-component column vector; $\boldsymbol{D}(\boldsymbol{Q},t)$ is a positive semi-definite 3×3 matrix.

In the stochastic simulation technique, instead of solving Eq. (5) directly, the polymer configuration $\boldsymbol{Q}(t)$ is determined by using an equivalent SDE which is given by

$$d\boldsymbol{Q}(t)=\boldsymbol{A}(\boldsymbol{Q}(t),t)dt+\boldsymbol{B}(\boldsymbol{Q}(t),t)\cdot d\boldsymbol{W}(t) \quad (6)$$

where $\boldsymbol{W}(t)$ is a 3-component column vector which is a Wiener process with mean $\langle \boldsymbol{W}_i(t)\rangle=0$ and covariance $\langle \boldsymbol{W}_i(t)\boldsymbol{W}_j(t')\rangle=\delta_{ij}\ \min(t,t')$; $\boldsymbol{B}(\boldsymbol{Q},t)$ is a 3×3 matrix and $\boldsymbol{D}(\boldsymbol{Q},t)=\boldsymbol{B}(\boldsymbol{Q},t)\boldsymbol{B}^T(\boldsymbol{Q},t)$. Stochastic theory shows that in general, the square-root tensor $\boldsymbol{B}$ is not unique because of the symmetry of matrix $\boldsymbol{D}$ (Ottinger, 1996). There are several schemes to evaluate the tensor $\boldsymbol{B}$, among of them is the Cholesky decomposition which is generally employed. In the present work, $\boldsymbol{B}$ is specifically given in closed form for each of the FENE and FENE-P models as shown in later sections. The theory also shows that although the trajectories obtained from the SDE are different for various choices of the tensor $\boldsymbol{B}$, all transition probabilities and then their averages are identical (more details can be found in Ottinger (1996), for example).

In polymeric fluids, for a given kinetic model of polymer molecules, the solution of Eq. (6) at each time t_i (the time discretization) is obtained by the simulation of the configuration of the model, which starts from a given probability distribution function of the configuration at t_o. The drift and diffusion terms $\boldsymbol{A}$ and $\boldsymbol{B}$ respectively of Eq. (6) depend on the given kinetic models. The numerical integration of the SDE (6) can be carried out using different schemes (Ottinger, 1996; Kloeden *et al.*, 1997; Kloeden and Platen, 1997; Gardiner, 1990; Gihman and Skorohod, 1974). In this paper, the explicit Euler integration scheme is employed. The SDE's and their numerical solution for some kinetic models are presented in the next subsection.

4.1. FENE dumbbell model

In the kinetic dumbbell models, the polymer solution is considered as a suspension of a great number of non-interacting dumbbells. Each dumbbell consists of two Brownian beads with the friction coefficient ζ, which are connected together by a spring as shown in Fig. 1. The configuration of a dumbbell is completely described by the length and orientation of the vector $\boldsymbol{Q}$ connecting the two beads. In a Hookean dumbbell model (not used in this paper) the linear spring force is realistic only for small deformation from the static equilibrium configuration and the extent of the dumbbell's stretch is not limited. This unphysical behaviour is overcome by the FENE model which plays an important role in non-linear rheological phenomena. Neglecting the external forces, the diffusion Eq. (5) corresponding to the FENE model can be expressed as (Ottinger, 1996; Laso *et al.*, 1999; Bird *et al.*, 1987)

$$\rho\frac{\partial}{\partial t}\psi(\boldsymbol{Q},t)=\frac{2}{\zeta}\frac{\partial}{\partial \boldsymbol{Q}}\cdot F\psi-\frac{\partial}{\partial \boldsymbol{Q}}\cdot[\boldsymbol{\kappa}\cdot\boldsymbol{Q}]\psi+\frac{2kT}{\zeta}\frac{\partial}{\partial \boldsymbol{Q}}\cdot\frac{\partial}{\partial \boldsymbol{Q}}\psi \quad (7)$$

where $\boldsymbol{\kappa}=(\nabla\boldsymbol{u})^T$ is the transpose of the velocity gradient which can be a function of time, but not position (i.e. locally homogenous flows at the dumbbell (Bird *et al.* 1987, §13.2)). The velocity gradient tensor is calculated analytically from the velocity field which is approximated by TPS-RBFN (see §5 and step (d) of §6 for more details). In the present work, the local homogeneity of the flow around each dumbbell can naturally be assumed in an arbitrarily small volume around the dumbbell. The spatially constant velocity gradient takes the value computed at the dumbbell centre of mass position. The FENE spring force $\boldsymbol{F}$ is given by (Bird *et al.*, 1987; Herrchen and Ottinger, 1997)

$$\boldsymbol{F}=\frac{H}{1-\left(\frac{\boldsymbol{Q}}{Q_o}\right)^2}\boldsymbol{Q} \quad (8)$$

where Q^o is the maximum possible spring length. The SDE corresponding to the FENE model is now given by

$$d\boldsymbol{Q}(t)=\left[\boldsymbol{\kappa}(t)\cdot\boldsymbol{Q}(t)-\frac{2H}{\zeta}\cdot\frac{\boldsymbol{Q}(t)}{1-\left(\frac{\boldsymbol{Q}(t)}{Q_o}\right)^2}\right]dt+\sqrt{\frac{4kT}{\zeta}}d\boldsymbol{W}(t) \quad (9)$$

where $\boldsymbol{W}(t)$ accounts for the random displacement of the beads due to thermal motion; T is the absolute temperature and k is Boltzmann constant.

Let $\boldsymbol{Q}_i$ be an approximation of $\boldsymbol{Q}(t)$ at time t_i, $\Delta t=t_{(i+1)}-t_i$. The solution from the explicit Euler integration scheme is written as follows

$$\boldsymbol{Q}_{(i+1)}=\boldsymbol{Q}_i+\left(\boldsymbol{\kappa}_i\cdot\boldsymbol{Q}_i-\frac{2H}{\zeta}\cdot\frac{\boldsymbol{Q}_i}{1-\left(\frac{\boldsymbol{Q}_i}{Q_o}\right)^2}\right)\Delta t+\sqrt{\frac{4kT}{\zeta}}\Delta\boldsymbol{W}_i \quad (10)$$

The dimensionless forms of Eqs. (9) and (10) are written as follows (by dividing by $\sqrt{kT/H}$)

$$d\boldsymbol{Q}'(t) = \left[\boldsymbol{\kappa}(t)\cdot\boldsymbol{Q}'(t) - \frac{1}{2\lambda_H}\cdot\frac{\boldsymbol{Q}'(t)}{1-\frac{\boldsymbol{Q}'^2}{b}} \right] dt + \sqrt{\frac{1}{\lambda_H}}\, d\boldsymbol{W}(t) \tag{11}$$

$$\boldsymbol{Q}'_{(i+1)} = \boldsymbol{Q}'_i + \left(\boldsymbol{\kappa}_i\cdot\boldsymbol{Q}'_i - \frac{1}{2\lambda_H}\cdot\frac{\boldsymbol{Q}'_i}{1-\frac{\boldsymbol{Q}'^2_i}{b}} \right)\Delta t + \sqrt{\frac{\Delta t}{\lambda_H}}\,\boldsymbol{W}_i \tag{12}$$

$\boldsymbol{Q}'_i = \boldsymbol{Q}_i\sqrt{H/kT}$ is the dimensionless connector vector at t_i; $\lambda_H = \zeta/(4H)$ is the relaxation time of dumbbells; $b = HQ_o^2/kT$ is the square of the maximum extension of the dimensionless connector vector $\boldsymbol{Q}'$. Thus in the FENE dumbbell model, the connector vector cannot be stretched beyond a maximum value of $\sqrt{b}$ in the dimensionless sense (Laso and Ottinger, 1993). The components of the random vector $\boldsymbol{W}_i$ are independent Gaussian variables with zero mean and Δt variance. Because of the non-linearity of the spring force, this model has no corresponding closed form constitutive equation for the polymeric stress tensor and therefore it cannot be solved with the traditional macroscopic approaches.

Based on the polymer configuration Eq. (12), the dimensionless form of stress tensor of polymer contribution at the time t_i can be determined as follows (Ottinger, 1996; Bird *et al.*, 1987; Herrchen and Ottinger, 1997)

$$\boldsymbol{\tau}_i^p = -nkT\left(\left\langle \frac{\boldsymbol{Q}'_i\boldsymbol{Q}'_i}{1-\frac{\boldsymbol{Q}'^2_i}{b}} \right\rangle - \boldsymbol{I} \right) \tag{13}$$

where n is number of dumbbells per unit volume of solution.

4.2. FENE-Peterlin (FENE-P) dumbbell model

The FENE-P model is based on the FENE dumbbell model in which the term $\boldsymbol{Q}^2/Q_o^2$ in the denominator of spring force shown in Eq. (8) is replaced by its average $\langle \boldsymbol{Q}^2/Q_o^2 \rangle$. The spring force $\boldsymbol{F}$ is rewritten as follows (Bird *et al.*, 1987; Herrchen and Ottinger, 1997; Keunings, 1996)

$$\boldsymbol{F} = \frac{H}{1-\left\langle \frac{\boldsymbol{Q}^2}{Q_o^2} \right\rangle}\boldsymbol{Q}. \tag{14}$$

In this case, the dimensionless form of the polymer configuration and the contribution to stress are given as follows, respectively,

$$\boldsymbol{Q}'_{(i+1)} = \boldsymbol{Q}'_i + \left(\boldsymbol{\kappa}_i\cdot\boldsymbol{Q}'_i - \frac{1}{2\lambda_H}\cdot\frac{\boldsymbol{Q}'_i}{1-\frac{\langle \boldsymbol{Q}'^2 \rangle}{b}} \right)\Delta t + \sqrt{\frac{\Delta t}{\lambda_H}}\,\boldsymbol{W}_i \tag{15}$$

$$\boldsymbol{\tau}_i^p = -nkT\left(\frac{\langle \boldsymbol{Q}'_i\boldsymbol{Q}'_i \rangle}{1-\frac{\langle \boldsymbol{Q}'^2_i \rangle}{b}} - \boldsymbol{I} \right). \tag{16}$$

The average which appears in the denominator of Eqs. (15) and (16) is calculated over the number of dumbbells in a small local domain where the dumbbells are located. From Eq. (15), it can be seen that the length of connector vectors $\boldsymbol{Q}'$ could become greater than the maximum allowable limit $\sqrt{b}$ during the simulation (Laso and Ottinger, 1993; Keunings, 1996). In the present work, this unphysical situation is corrected by contracting the unphysical value as follows $\|\boldsymbol{Q}'_c\| = \|\boldsymbol{Q}'_c\| - mod(\|\boldsymbol{Q}'\|, \sqrt{b})$. The "reflecting" method of Laso and Ottinger (1993) is a special case in which the length of $\boldsymbol{Q}'$ satisfies: $\sqrt{b} < \|\boldsymbol{Q}'\| < 2\sqrt{b}$.

At time step $(i + 1)$, the computed stress tensor $\boldsymbol{\tau}_{i+1}^p$ is then employed to get the solution of the velocity field $\boldsymbol{u}$ from the governing PDE's (1) and (2) which are solved by a RBFN-based numerical method presented in the next section.

5. Radial basis function networks for solving the continuity and momentum equations

Recently, the application of RBFNs in numerical solution of PDE's have brought interesting results (Kansa, 1990; Zerroukat *et al.*, 1998; Mai-Duy and Tran-Cong, 2001). Comparing many available interpolation methods for scattered data, Franke (1982) ranked Multiquadric RBF (MQ-RBF) of Hardy (1971) and Thin Plate Splines RBF (TPS-RBF) of Duchon (1976) as superior in accuracy and both of these RBFs are employed in the present work. Since TPS-RBFN has the advantage of containing no adjustable width parameter, it is a preferred choice in this paper.

5.1. Radial basis function network interpolation

In principle, it is possible to approximate any smooth function with radial basis function networks having a single hidden layer architecture. The present work uses the linear RBF network with one hidden layer of RBFs where the function $f(\boldsymbol{x})$ is decomposed into m fixed RBFs as

$$f(\boldsymbol{x}) = \sum_{j=1}^{m} w^j h^j(\boldsymbol{x}) \tag{17}$$

where w^j is the synaptic weight and h^j is the chosen radial basis function corresponding to the j^{th} neuron. Usually $m \leq n$ (Haykin, 1999) where n is the number of input data points $(\boldsymbol{x}_i, \widehat{y}_i)$; $\boldsymbol{x}_i$ is the coordinate of the i^{th} collocation point ($\boldsymbol{x}_i$ is a scalar in the case of 1-dimensional space) and $\widehat{y}_i$ is the desired value of function f at the collocation point $\boldsymbol{x}_i$. After the training process is completed, a set of weights corresponding to the chosen radial basis functions is obtained. It is important to recognise that the RBF networks are function approximating networks and not learn-

ing networks in the present context. Therefore, for a given discretisation, there is only one "training pattern" and the network weights are found in a single general linear least square procedure (Mai-Duy and Tran-Cong, 2001). The partial derivatives of $f(\boldsymbol{x})$ can be calculated analytically as follows

$$\frac{\partial^k f(\boldsymbol{x})}{\partial x_i \ldots \partial x_n} = \sum_{j=1}^{m} w^j \frac{\partial^k h^j}{\partial x_i \ldots \partial x_n}. \tag{18}$$

As mentioned above, the RBF's h^j employed here are either MQ-RBF or TPS-RBF which are given by

$$h^j(\boldsymbol{r}) = h^j(\|\boldsymbol{x}-\boldsymbol{c}^j\|) = \sqrt{r^2+a^{(j)2}} \tag{19}$$

for the MQ-RBF, and

$$h^j(\boldsymbol{r}) = h^j(\|\boldsymbol{x}-\boldsymbol{c}^j\|) = r^{2m}\log(r), \quad m = 1,2,\ldots \tag{20}$$

for the TPS-RBF.

The corresponding first order derivatives are given by

$$\frac{\partial h^j}{\partial x_i} = \frac{x_i - c_i^j}{\sqrt{r^2+a^{(j)2}}} \tag{21}$$

for the MQ-RBF, and

$$\frac{\partial h^j}{\partial x_i} = r^{2(m-1)}(x_i - c_i^j)(2m\log(r)+1) \tag{22}$$

for the TPS-RBF.

The corresponding second order derivatives are given

$$\frac{\partial^2 h^j}{\partial x_i \partial x_1} = \frac{\chi(r) - (x_i - c_i^j)(x_1 - c_1^j)}{\sqrt{(r^2+a^{(j)2})^3}},$$
$$\chi(r) = x^2 + a^{(j)2} \quad \forall i = 1,$$
$$\chi(r) = 0 \quad \forall i \neq 1 \tag{23}$$

for the MQ-RBF, and

$$\frac{\partial^2 h^j}{\partial x_i \partial x_1} = 2r^{2(m-2)}(x_i - c_i^j)(x_1 - c_1^j)[2m(m-1)\log(r) + (2m-1)] + \chi(r)$$
$$\chi(r) = r^{2(m-1)}(2m\log(r)+1) \quad \forall_i = 1$$
$$\chi(r) = 0 \quad \forall i \neq 1 \tag{24}$$

for the TPS-RBF where $\boldsymbol{r} = (\boldsymbol{x} - \boldsymbol{c}^j)$ and $r = \|(\boldsymbol{x}-\boldsymbol{c}^j)\|$ is the Euclidean norm of $\boldsymbol{r}$; $\{\boldsymbol{c}^j\}$is a set of centres that can be chosen from among the data points; $a^j > 0$ is called the width of the j^{th} RBF (Haykin, 1999). The accuracy of the MQ-RBF approximation is very dependent on the width of the RBF (Kansa, 1990; Park and Sandberg, 1991; Carlson and Foley, 1991), whose choice is still an open question.

In the present work, the set of centres is the same as the set of training points. The width a^j is computed according to Orr (1997) as follows

$$a^j = kd^j \tag{25}$$

where d^j is the distance from the j^{th} centre to the nearest centre; k is a chosen coefficient.

Since the MQ-RBF is C^∞-continuous, it can be employed directly. In the case of TPS-RBF, it is C^{2m-1}-continuous, the power index m must be appropriately chosen for a given partial differential operator (Zerroukat *et al.*, 1998). In the present work, the TPS-RBF with $m \geq 2$ is chosen to satisfy the continuity condition.

The training of the linear model Eq. (17), given a training set of p collocation points $\{(\boldsymbol{x}_i, \widehat{y}_i)\}_{i=1}^p$, can be achieved via the minimisation of a cost function based on the sum of squared errors

$$C(\boldsymbol{w}) = \sum_{i=1}^{p} (\widehat{y}_i - f(x_i))^2. \tag{26}$$

Furthermore, in order to counter the effect of over-fitting, a roughness penalty term can be added to the cost function to produce

$$C(\boldsymbol{w}, \Lambda) = \sum_{i=1}^{p} (\widehat{y}_i - f(x_i))^2 + \Lambda \sum_{j=1}^{m} w^{(j)2} \tag{27}$$

where Λ is the global regularisation parameter. The minimisation of the cost function Eq. (26) (without regularisation) or Eq. (27) (with a given regularisation parameter Λ) yields an optimal weight vector $\boldsymbol{w} = [\widehat{w}^1\ \widehat{w}^2 \ldots \widehat{w}^m]^T$ as follows

$$\boldsymbol{w} = \boldsymbol{A}^{-1}\boldsymbol{H}^T\widehat{\boldsymbol{y}} \tag{28}$$

where $\boldsymbol{H}$ is the design matrix with $H_i^j = h^j(x_i)$ and vector $\widehat{\boldsymbol{y}} = [\widehat{y}_1\ \widehat{y}_2 \ldots \widehat{y}_p]^T$ is the p-dimensional vector of training output values. $\boldsymbol{A}^{-1} = (\boldsymbol{H}^T\boldsymbol{H})^{-1}$ (without regularisation) $\boldsymbol{A}^{-1} = (\boldsymbol{H}^T\boldsymbol{H} + \Lambda\boldsymbol{I})^{-1}$ (with regularisation) and $\boldsymbol{I}$ is the identity matrix (Tran-Canh and Tran-Cong, 2002; Orr, 1997,1999).

Using the RBFN-based approximation, the function $f(\boldsymbol{x})$ as given in Eq. (17) is determined after the training and its derivatives can be calculated analytically in terms of basis functions as mentioned in Eq. (18)-Eq. (24).

5.2. Time integration of the momentum conservation equation by collocation and RBFN method

This section describes the RBFN-based numerical method employed to solve the continuity and the momentum equations in which the velocity field $\boldsymbol{u}$ is considered as an unknown and the polymer contributed stress $\boldsymbol{\tau}^p$ is already computed by the SST as described in §2–4. Specifically, the start-up planar Couette flows is used to explain the method.

5.2.1. Governing equation, boundary conditions and initial conditions

For the start-up planar Couette flow problem, a catersian coordinate system is chosen as shown in Fig. 2. For $t < 0$, the fluid is at rest. At $t = 0$, the lower plate starts to move with a constant velocity V. No-slip condition is assumed at

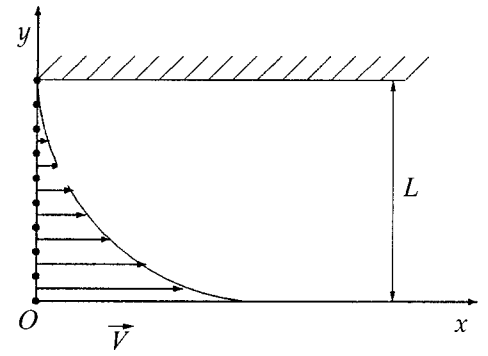

Fig. 2. The start-up planar Couette flow problem: the bottom plate moves with a constant velocity V, the top plate is fixed; no-slip boundary conditions apply at the fluid-solid interfaces. The collocation point distribution is only schematic.

the walls, following Mochimaru (1983).

A velocity field that satisfies the equation of continuity (2) is given by

$$u = u_x = u_x(y,t), \quad u_y = 0, \quad u_z = 0 \tag{29}$$

In the present problem, it is not necessary to calculate the pressure field (Laso and Ottinger, 1993; Mochimaru, 1983) and the momentum Eq. (4) is rewritten as follows

$$\rho\frac{\partial u}{\partial t} = \eta_s\frac{\partial^2 u}{\partial y^2} - \frac{\partial \tau_{yx}^p}{\partial y} \qquad y \in \Omega \tag{30}$$

where y and t are the space and time coordinates; ρ is the density of the fluid; η_s is the solvent viscosity; $\tau_{yx}^p(y,t)$ is the polymer-contributed stress. In the more general situation the pressure would have to be calculated.

Eq. (30) is subjected to Dirichlet boundary conditions as follows

$$\begin{aligned} &u(0,t) = V \quad \forall t > 0, \\ &u(L,t) = 0 \quad \forall t > 0 \end{aligned} \tag{31}$$

and the initial conditions

$$u(0,0) = V, \quad u(y,0) = 0, \quad \forall y \neq 0 \tag{32}$$

The shear stress τ_{yx}^p at a time step is considered as a known function of y and calculated from the previous step by Brownian simulation technique already described. Its derivative $\frac{\partial \tau_{yx}^p}{\partial y}$ is approximated by a RBFN-based method as presented in §5.1.

The PDE (30), subject to Eq. (31) and Eq. (32), can be solved by a RBFN-based numerical method which is described in the next subsection.

5.2.2. Solution of differential equations by collocation and RBFN method

Using the standard implicit approximation and rearranging the terms, Eq. (30) can be written as follows (Kansa, 1990; Zerroukat *et al.*, 1998; Constantinides and Mostoufi, 1999)

$$u^{n+1} + \alpha\frac{\partial^2 u^{n+1}}{\partial y^2} = u^n + \beta\frac{\partial^2 u^n}{\partial y^2} + \Delta t K^{n+1/2} \tag{33}$$

where Δt is a uniform time step size; let $t_n = t_{n-1} + \Delta t$, $u^n = u(y, t_n)$; $\alpha = -\theta\Delta t\ \frac{\eta_s}{\rho}$; $\beta = (1-\theta)\Delta t\frac{\eta_s}{\rho}$ with $0 \le \theta \le 1$; K = $\frac{1}{\rho}\cdot\frac{\partial \tau_{yx}^p}{\partial y}$; and (Constantinides and Mostoufi, 1999)

$$K^{n+1/2} = \frac{1}{2}(K^{n+1} + K^n) \tag{34}$$

where $K^n = K(t_n)$ and K^{n+1} is approximated by backward difference as follows

$$K^{n+1} = (K^n + \dot{K}^n \Delta t) = 2K^n - K^{n-1} \tag{35}$$

where $\dot{K}^n$ is the gradient of K at t_n. Using (34) and (35), (33) is rewritten by

$$u^{n+1} + \alpha\frac{\partial^2 u^{n+1}}{\partial y^2} = u^n + \beta\frac{\partial^2 u^n}{\partial y^2} + \frac{\Delta t}{2}(3K^n - K^{n-1}) \tag{36}$$

Thus Eq. (36) is the time discretization of the PDE (30) in which the terms on the RHS are determined from the previous steps. The first and second terms on the RHS are determined from a TPS-RBFN-based approximation of the current velocity field. The third term is obtained from a TPS-RBFN-based approximation of the data of the Brownian simulation process.

Specifically, to start the process, Eq. (36) is rewritten as follows

$$u^1 + \alpha\frac{\partial^2 u^1}{\partial y^2} = u^0 + \beta\frac{\partial^2 u^0}{\partial y^2} + \frac{3K^0}{2}\Delta t \tag{37}$$

where $K^0 = \frac{1}{\rho}\frac{\partial \tau_{yx}^p}{\partial y}\Big|^0$. It can be seen that the first term on the RHS of (37) is the initial condition of the problem.

In the present work, Eq. (36) with the boundary conditions (31) is solved for u at the time step (n+1) using the linear least square principle. The sum of squared errors corresponding to the first step is given by

$$SSE(1) = \sum_{y_i \in \Omega}\left[\left(u^1(y_i) + \alpha\frac{\partial^2}{\partial y^2}u^1(y_i)\right) - \left(u^0(y_i) + \beta\frac{\partial^2}{\partial y^2}u^0(y_i) + \frac{3}{2}\Delta t K^0(y_i)\right)\right]^2 + [u^0(0) - V]^2 + [u^0(L)]^2 \tag{38}$$

where Ω is the domain under consideration. u^1, τ_{yx}^p and their derivatives in Eq. (38) are approximated by either MQ-RBFNs (Eq. 17, Eq. 18, Eq. 19 and Eq. 23) or TPS-RBFNs (Eq. 17, Eq. 18, Eq. 20 and Eq. 24). Note that in the case of 1-D problem under consideration, y_i's are internal collocation points, $y_o = 0$ and $y_1 = L$ are boundary collocation points. Generally, at time level (n+1), the sum of squared errors is

$$SSE(n+1)=\sum_{y_i\in\Omega}\left[\left(u^{n+1}(y_i)+\alpha\frac{\partial^2}{\partial y^2}u^{n+1}(y_i)\right)-\left(u^n(y_i)+\beta\frac{\partial^2}{\partial y^2}u^n(y_i)\right.\right.$$

$$\left.\left.+\frac{\Delta t}{2}(3K^n(y_i)-K^{n-1}(y_i))\right)\right]^2+[u^n(0)-V]^2+[u^n(L)]^2 \quad (39)$$

In the general case, the set of collocation points consists of the internal data and boundary data points. The collocation points can be distributed randomly or regularly. In this paper, the collocation points are arranged on the regular grid and coincident with RBF centres. This choice gives the best results according to Kansa (1990), Zerroukat *et al.* (1998) and Mai-Duy and Tran-Cong (2001). A system of linear algebraic equations is obtained in terms of the unknown weights as shown in Eq. (28) and rewritten as follows

$$\boldsymbol{A}\boldsymbol{w}=\boldsymbol{H}^T\widehat{\boldsymbol{y}} \quad (40)$$

where $\boldsymbol{A}$ is the variance matrix and described in §5.1. Here, each row of the design matrix $\boldsymbol{H}$ contains the values of the RBF corresponding to the terms $u^1(y_i)+\alpha\frac{\partial^2 u^1(y_i)}{\partial y^2}$; $\widehat{\boldsymbol{y}}$ is a column vector whose elements correspond to the terms $u^1(y_i)+\beta\frac{\partial^2 u^0(y_i)}{\partial y^2}+\frac{3}{2}\Delta tK^0(y_i)$ and $\boldsymbol{w}$ is the vector of weights. The velocity field is thus described by the RBFNs once the sets of weights are calculated.

The numerical solution of the velocity field $\boldsymbol{u}^1$ from Eq. (38) (in the least square sense) is the starting point for the solution of (39) at a general time step. The process continues until the steady state or a desired time is reached. The time discretisation is based on the Crank-Nicolson implicit method with $\theta=0.5$ which reduces the total volume of calculation and is convergent and stable for a large range of $\frac{\Delta t}{\Delta y^2}$ (Smith, 1978; Carnahan *et al.*, 1969).

6. Algorithm of the CVFNNSS procedure

The general macro-microscopic approach mentioned in §3 can now be described in a more detailed algorithm as follows.

a. Start with a given initial velocity condition, generate a set of collocation points and an initial velocity field is approximated by RBF networks;

b. Generate an ensemble of homogenously distributed dumbbells over the flow domain. This initialisation of the polymer configuration field is based on the known equilibrium distribution function which is a three dimensional Gaussian distribution with zero mean and unit covariance (Ottinger, 1996; Bird *et al.*, 1987);

c. Generate local volumes surrounding the collocation points. The local volumes are chosen such that each dumbbell is accounted for in one of these local volumes;

d. After the current velocity field is approximated by RBF networks, determine the velocity gradient field by calculating directly the gradient of the approximated velocity field for individual dumbbells;

e. Calculate the polymer configuration field (the connector vectors of the dumbbell ensemble) using the method described in §4. The velocity of the centre of mass of each dumbbell is considered to be equal to the point-wise local fluid velocity;

f. Determine the local stress tensor by taking the ensemble average of the polymer configuration on each local volume and assign this stress to the collocation point associated with this volume. The stress is then approximated globally on the whole domain by RBF networks which are the ultimate description of the stress field. This global approximation procedure smooths the piecewise continuous stress field with a globally continuous function. This could be achieved by either TPS-RBFNs or MQ-RBFNs. However, the former was proved to have superior smoothing characteristics (Beatson and Light, 1997) and hence is used in the present work;

g. With the stress field just obtained, solve the set of conservation equations for the new velocity field using a meshfree RBFN method as described in §5;

h. Terminate the simulation when either the desired time or steady state is reached. The latter is determined by a convergence measure for either the velocity field or the stress field between two consecutive iterations which is defined for velocity field by

$$CM=\sqrt{\frac{\sum_{1}^{N}\sum_{i=1}^{d}(u_i^n-u_i^{n-1})^2}{\sum_{1}^{N}\sum_{i=1}^{d}(u_i^n)^2}}<tol \quad (41)$$

where d is the number of dimension 1 in the present work); tol is a preset tolerance; u_i is the i component of the velocity at a node; N is the total number of collocation points and n is the iteration number. Convergence is also checked for the shear stress and the first normal stress difference;

i. Return to step (d) for the next time level.

7. Numerical examples

The aim of the present work is to report an initial assessment of the validity and efficiency of the present meshless method and therefore the start-up planar Couette flow is considered using two kinds of kinetic dumbbell models: the FENE and FENE-P. The problem, already described in §5.2.1 and Fig. 2, was solved using the FENE-P model by Mochimaru (1983), and FENE/FENE-P by Laso and Ottinger (1993) while Fan (1985) provided a steady state solution using the FENE model. In order to compare the present results with those from Mochimaru (1983), Laso

and Ottinger (1993), the same number of dumbbells M = 50000 is homogeneously distributed into the domain and the same non-dimensionlisation scheme as in Laso and Ottinger (1993) is used. The non-interacting dumbbells are neutrally suspended in a Newtonian solvent of known viscosity η_s, density ρ and the resultant material is characterized by the relaxation time λ_H. The dimensionless gap L = 1, moving plate velocity V = 1 and zero-shear-rate viscosity $\eta_o = \eta_s + \eta_p = 1$. A set of N collocation points is generated in the volume either randomly or regularly. For the comparison with others methods, in this simple geometry the local volumes are chosen line segments of equal length $L/(N\text{-}1)$ except the two volumes near the boundaries. In this work, the convergence measure is set at 10^{-4} and the simulation is continued for $t \geq 0$ until the flow reaches the steady state.

7.1. Start-up planar Couette flow with the FENE model

The FENE model has no closed-form constitutive equation and the problem was solved recently by Laso and Ottinger (1993) using the CONNFFESSIT approach. In this work, as in Laso and Ottinger (1993), the parameters are: 50000 dumbbells, 41 collocation points, $\rho = 1.2757$, $\lambda_H = 49.62$, $b = 50$, $\eta_s = 0.0521$, $\Delta t = 10^{-2}$ ($\Delta t = 10^{-4}$ in Laso and Ottinger (1993)). The numerical solution by the present method confirms the velocity overshoot of viscoelastic fluids and is in complete agreement with the findings of Laso and Ottinger (1993).

Fig. 3 describes the evolution of the velocity profile,

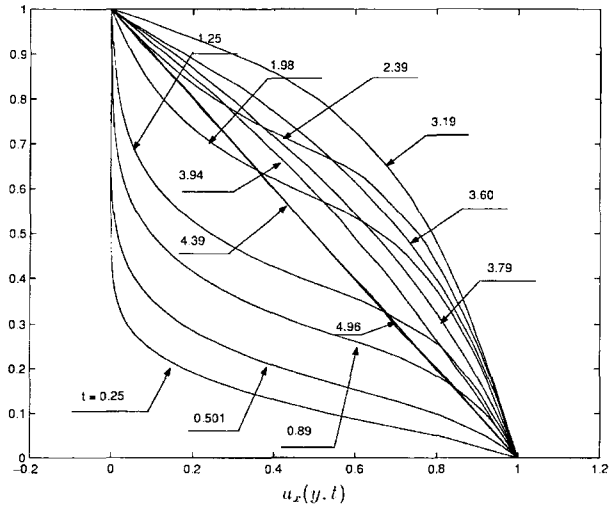

Fig. 3. The start-up planar Couette flow problem using the FENE dumbbell model: the parameters of the problem are number of dumbbells M=50000, number of collocation points N=41, λ_H=49.62, b=50, η_S=0.0521 and Δt=10^{-2}. The velocity profile with respect to location y at different times shows velocity overshoot but hardly any oscillation.

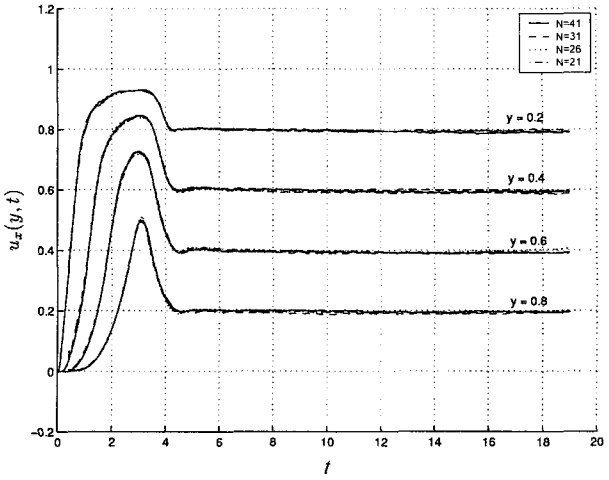

Fig. 4. The start-up planar Couette flow problem using the FENE dumbbell model: the parameters are same as in Fig. 3. The influence of the number of collocation points on the time evolution of the velocity at locations y=0.2, y=0.4, y=0.6 and y=0.8.

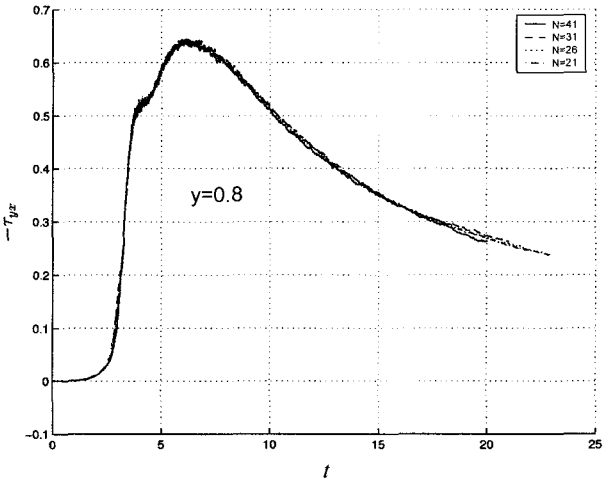

Fig. 5. The start-up planar Couette flows using the FENE model: the parameters other than N are shown in Fig. 3. The evolution of shear stress at the location y=0.8 with respect to time for N=41, 31, 26 and 21.

which shows that velocity undershoot is insignificant in comparison with overshoot. Fig. 4 shows that typical time evolutions of the velocity at four locations $y = 0.2$, $y = 0.4$, $y = 0.6$ and $y = 0.8$ do not differ significantly for the cases $N = 41$ and 31, indicating that $N = 31$ is an adequate number of collocation points. Fig. 4 also shows that velocity overshoot occurs sooner in fluid layers nearer to the moving wall.

Figs. 5 and 6 show a typical evolution of the shear stress and the first normal stress difference, respectively, at locations $y = 0.8$ for the cases of N = 41, 31, 26 and 21 collocation points. On the other hand, Fig. 7 and Fig. 8 depict

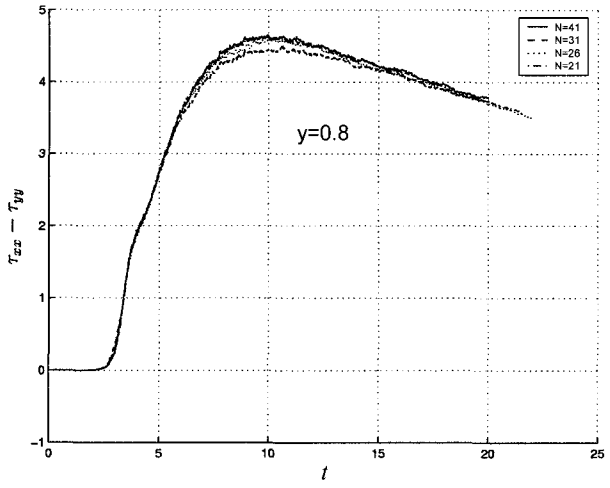

Fig. 6. The start-up planar Couette flows using the FENE model: the parameters other than N are the same as shown in Fig. 3. The evolution of the first normal stress difference at location y=0.8 with respect to time for N=41, 31, 26 and 21.

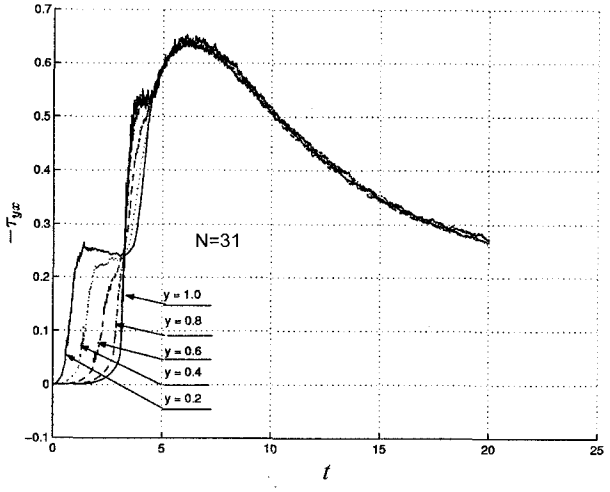

Fig. 7. The start-up planar Couette flows using the FENE model: the parameters are the same as shown in Fig. 3 except that the number of collocation points is 31. The evolution of shear stress at locations y=0.2, y=0.4, y=0.6, y=0.8 and y=1.0 with respect to time.

The evolution of shear stress and the first normal stress difference, respectively, at locations $y = 0.2$, $y = 0.4$, $y = 0.6$ and $y = 0.8$ using $N = 31$. The stress response is sharper near the moving wall which is consistent with the velocity overshoot behaviour.

The time-step size Δt influences the accuracy of the microscopic stochastic integration. Generally, the larger is the time-step size, the bigger is the mean error of solution of SDE's (9) or (11). However, when Δt is very small the variance may be large due to round-off errors and can destroy the result (Kloeden *et al.*, 1997, Kloeden and

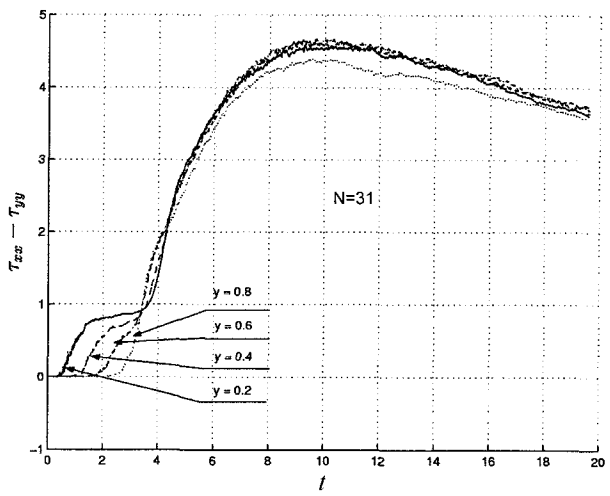

Fig. 8. The start-up planar Couette flows using the FENE model in the present CVFNNSS method: the parameters are the same as shown in Fig. 3 except that the number of collocation points is decreased from 41 to 31. The evolution of the first normal stress differences at locations y=0.2, y=0.4, y=0.6 and y=0.8 with respect to time.

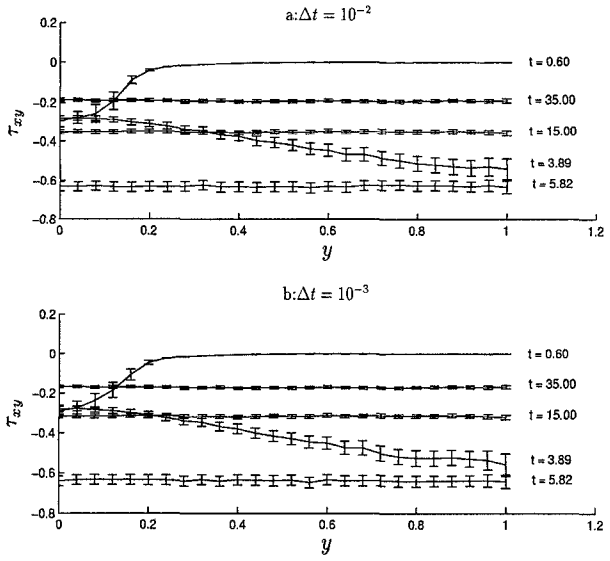

Fig. 9. The start-up planar Couette flows using the FENE model in the present CVFNNSS method: the shear stress profiles τ_{yx} and the statistical error bar with respect to location y at different times t=0.60, 3.89, 5.82, 15.00 and 35.00: the parameters are the same as shown in Fig. 3 except that the number of collocation points is equal to 26 for both time-step sizes (a) Δt=10^{-2} and (b) Δt=10^{-3}.

Platen, 1997). Furthermore, a very good agreement with the results of other methods is obtained by the present method with a coarse set of collocation points. Fig. 9 shows the shear stress profiles τ_{yx} and the statistical error

bars with respect to location y for a sampling of 120 computations using two time-step sizes, $\Delta t = 10^{-2}$ and 10^{-3}, and 26 collocation points, at the following times $t = 0.60$, 3.89, 5.82, 15.00 and 35.00. The results show that the statistical errors are small and stable at the steady state.

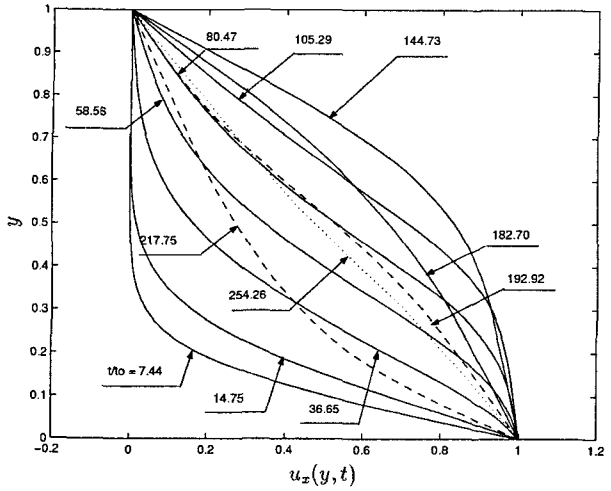

Fig. 10. The start-up planar Couette flow problem using the FENE-P dumbbell model in the present CVFNNSS method: the parameters are number of dumbbells M= 50000, number of collocation points N=41, λ_H=49.62, b=50, η_s=0.0521 and Δt=10^{-2}. The velocity profile with respect to location y at different times shows the strong velocity overshoots and undershoots. In this plot the time is non-dimensionlised with respect to the reference time t_o as defined in Mochimaru (1983) for easy comparison with the latter results.

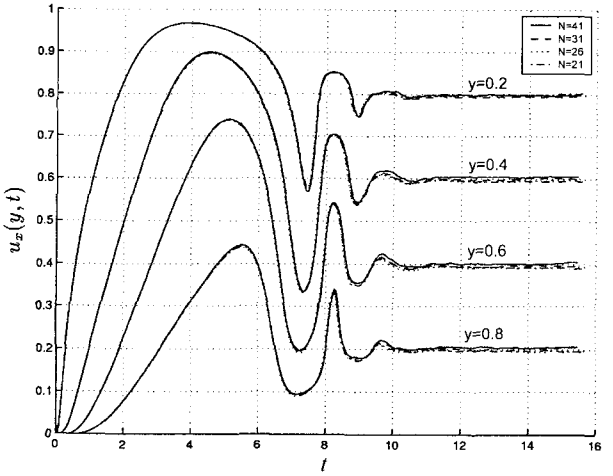

Fig. 11. The start-up planar Couette flow problem using FENE-P dumbbell model in the present CVFNNSS method: the parameters other than N are shown in Fig.10. The evolution of the velocity field with respect to time at locations y=0.2, y=0.4, y=0.6 and y=0.8 for the cases of N=41, 31, 26 and 21.

7.2. Start-up planar Couette flow with the FENE-P model

The start-up planar Couette flow problem using the FENE-P model was solved by Mochimaru (1983) where the macroscopic numerical approach made use of the constitutive equation derived from the kinetic theory of a dilute solution of the FENE-P dumbbells in a Newtonian fluid (e.g. equation (13.5-56) of Bird *et al.* (1987)). The problem with the same material parameters was also solved by Laso and Ottinger (1993) using the CONNFFESSIT method. Similarly, the problem is solved by the present CVFNNSS

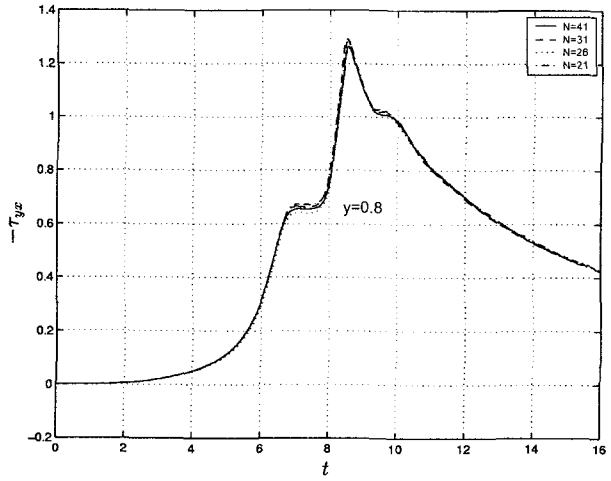

Fig. 12. The start-up planar Couette flows using the FENE-P model in the present CVFNNSS method: the parameters other than N are shown in Fig. 10. The evolution the shear stress at the location y=0.8 with respect to time for the cases of N=41, 31, 26 and 21.

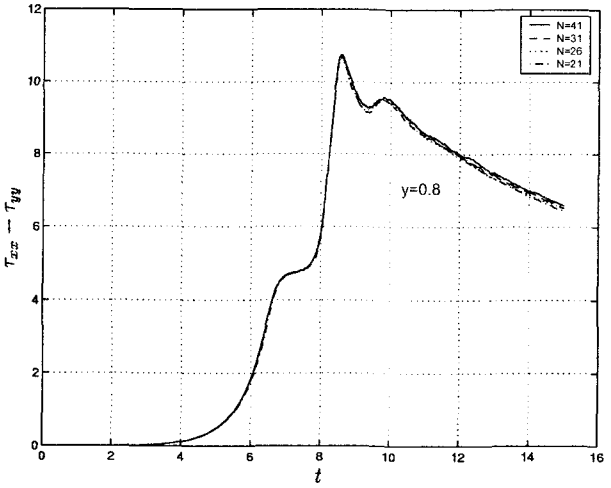

Fig. 13. The start-up planar Couette flows using the FENE-P model in the present CVFNNSS method: the parameters other than N are the same as shown in Fig. 10. The evolution of the first normal stress difference at location y=0.8 with respect to time for the cases of N=41, 31, 26 and 21.

method with the same parameters as in Mochimaru (1983), Laso and Ottinger (1993), i.e. ρ = 1.2325, λ_H = 49.62, b = 50, η_s = 0.050332. However the time increment Δt in the present method can be as high as 10^{-2} which appears to be an improvement in comparison with Laso and Ottinger (1993) where $\Delta t = 10^{-4}$. Fig. 10 and 11 show the evolution of velocity field which exhibits oscillatory transient behaviour. Keeping the number and distribution of dumbbells the same, the number of collocation points is varied from 21 to 41 (Figs. 11-13) to confirm that the obtained results are accurate. The present method are in excellent agreement with the theoretical results by Mochimaru (1983), Laso and Ottinger (1993) and the experimental results of Chow and Fuller (1985) confirm the velocity overshoots (Fig. 10-11) and stress propagation between the plates (Fig. 14-15).

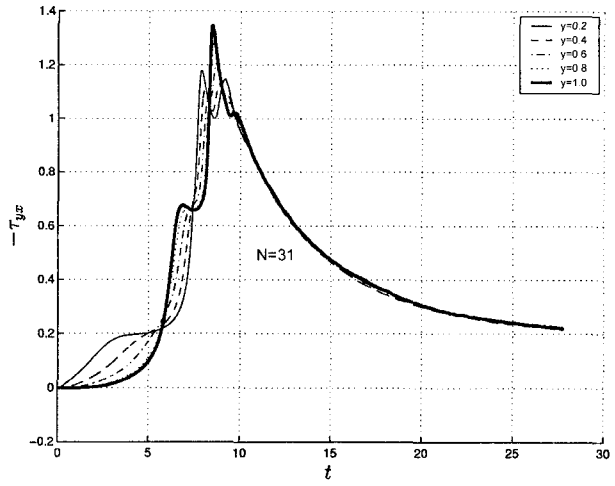

Fig. 14. The start-up planar Couette flows using the FENE-P model in the present CVFNNSS method: The parameters are the same as shown in Fig. 10 except that the number of collocation points is decreased from 41 to 31. The evolution of the shear stresses at locations y=0.2, y=0.4, y=0.6, y=0.8 and y=1.0 with respect to time.

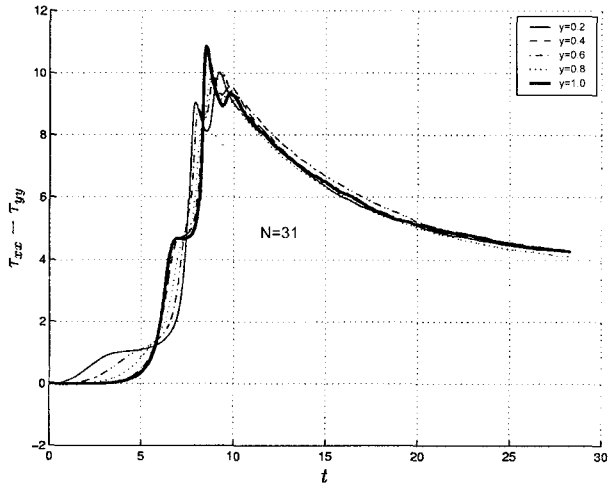

Fig. 15. The start-up planar Couette flows using the FENE-P model in the present CVFNNSS method: the parameters are the same as shown in Fig. 10 except that the number of collocation points is decreased from 41 to 31. The evolution of the first normal stress differences at locations y=0.2, y=0.4, y=0.6, y=0.8 and y=1.0 with respect to time.

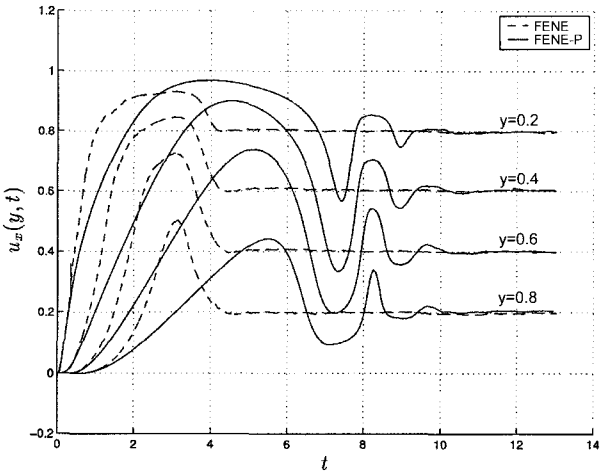

Fig. 16. The start-up planar Couette flows using FENE and FENE-P models in the present CVFNNSS method: the parameters are shown in Fig. 3 for the FENE model and Fig. 10 for the FENE-P model. Comparison of the velocity fields with respect to time at locations: y=0.2, y=0.4, y=0.6 and y=0.8.

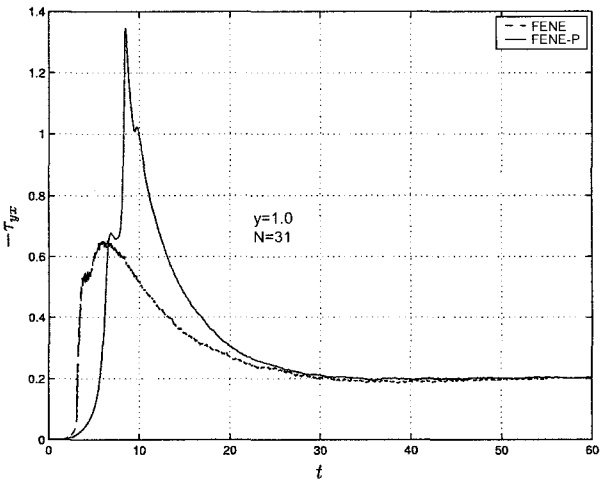

Fig. 17. The start-up planar Couette flow problem using FENE and FENE-P models in the present CVFNNSS method: the parameters are shown in Fig. 3 for the FENE model and Fig. 10 for the FENE-P model. Comparison of the shear stress at the fixed plate with respect to time between the two models.

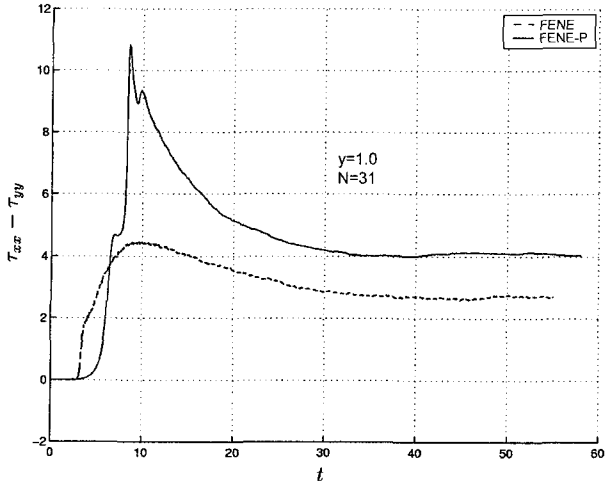

Fig. 18. The start-up planar Couette flow problem using the FENE and FENE-P models in the present CVFNNSS method: the parameters are shown in Fig. 3 for the FENE model and Fig. 10 for the FENE-P model. Comparison of the first normal stress difference at the fixed plate with respect to time between the two models.

7.3. Comparison between the FENE and FENE-P models

The comparison between the FENE and FENE-P models in planar Couette start-up flows is summarised in Figs. 16-18. Fig. 16 denotes the time development of velocity field at four locations $y = 0.2$, $y = 0.4$, $y = 0.6$ and $y = 0.8$ between the FENE and FENE-P models. It shows that there is a big difference in dynamic responses of two models, but the difference is non-significant after the flow reaches the steady state. Fig. 16 also shows that the duration of the velocity overshoot is much longer for the FENE-P model and the steady state seems to take much longer to be reached than for the FENE model. The strong oscillatory behaviour of the velocity and stress fields because of the linearisation of the FENE-P models is in excellent agreement with Laso and Ottinger (1993).

Fig. 17 depicts the difference of the evolution of shear stresses between the FENE and FENE-P models at the fixed plate with respect to time. It can be seen that the FENE-P model produces a maximum of the shear stress about twice the corresponding value for FENE, however the maximum value seems to take longer to be reached for the FENE-P model than for the FENE model. Furthermore, the asymtotic values of the stress are the same at the steady state in agreement with Laso and Ottinger (1993) and Herrchen and Ottinger (1997) and the steady state is reached in about the same time.

The comparison of the first normal stress difference between the FENE and FENE-P models at the fixed plate is shown in Fig. 18. The maximum values of the first normal stress difference seem to take the same time to be reached for both models, despite the delay in the wall shear stress maximum in the case of the FENE-P model. However, the values at the steady state are different although they reach the steady state at about the same time.

8. Conclusions

The present work has demonstrated a successful adaptation of the macro-micro approach introduced in the CONNFFESSIT method. The finite-element based macro-procedure of the CONNFFESSIT is replaced by the present meshless neural network-based procedure.

For the start-up Couette flow with the FENE and FENE-P models, a complete agreement on the typical flow features with the results of Mochimaru (1983) and Laso and Ottinger (1993) is obtained. The present CVFNNSS method retains the properties inherent in the CONNFFESSIT (Ottinger, 1996; Laso and Ottinger, 1993; Feigl *et al.*, 1995; Laso *et al.*, 1997, 1999) namely (i) easy handling of complex polymer models without closed form constitutive equation, (ii) easy switching between different models, (iii) realistic treatment of boundary conditions. Furthermore, the present CVFNNSS has the advantage of being a mesh-free numerical method where the domain discretization for the governing PDE's is simply an unstructured set of collocation points. Owing to the approximation characteristics of RBFNs, the initial conditions are represented in a more natural way. The use of TPS-RBFN based approximation results in a very smooth global stress tensor. For shear flows, the present CVFNNSS method appears to be much more stable than other methods reviewed here and becomes unstable only at $\Delta t = 5\text{e-}2$. Furthermore, with a coarse set of collocation points, the present method gives results with the similar accuracy in comparison with those from other schemes. However, these initial results are to be confirmed with more complex flows, e.g. elongational flows and/or fluids with more complicated dumbbell models in the future where numerical issues such as stochastic integration schemes, choice of collocation points could be expected to play a more critical role. The noise arising in the velocity field and specifically in the stress tensor (Fig. 5-8, Fig. 12-15 and Fig. 17-18) due to the Brownian motion can be drastically reduced by variance reduction methods (Ottinger *et al.*, 1997; Bovin and Picasso, 1999). Variance reduction methods will also be taken into account when the present method is implemented for higher dimensional problems in the next stage of investigation.

Acknowledgements

This work is supported by a Special USQ Research Grant, grant number of 179-442 and a grant of computing time from Australia Partnership for Advanced Computing (APAC) National Facility, grant number d72 to *T.* Tran-

Cong. D. Tran-Canh is supported by a USQ Scholarship. This support is gratefully acknowledged. The authors would like to thank Prof H.C. Ottinger and Prof M. Laso for their communications and the referees for their helpful comments.

References

Beatson, R.K. and W.A. Light, 1997, Fast evaluation of radial basis functions: methods for two-dimensional polyharmonic splines, *IMA J. Numerical Analysis* **17**, 343-372.

Belytschko, T., Y. Krongauz, D. Organ, M. Fleming and P. Krysl, 1996, Meshless methods: An overview and recent developments, *Comput. Methods Appl. Mech. Engrg.* **139**, 3-47.

Bird, R.B, C.F. Curtiss, R.C. Armstrong and O. Hassager, 1987, Dynamics of polymeric liquids, Vol 2, John Wiley & Sons, New-York.

Bovin, J. and M. Picasso, 1999, Variance reduction methods for CONNFFESSIT-like simulations, *J. Non-Newt. Fluid Mech.* **84**, 191-215.

Carlson, R.E. and T.A. Foley, 1991, The parameter R^2 in multiquadric interpolation, *Computers Math. Applic.* **21(9)**, 29-42.

Carnahan, B., H.A. Luther and J.O. Wilkes, 1969, Applied numerical methods, John Wiley & Sons, New-York.

Chow, A.W. and C.G. Fuller, 1985, Some experimental results on the developement of Couette flow for Non-Newtonian fluids, *J. Non-Newt. Fluid Mech.* **17**, 125-144.

Constantinides, A. and N. Mostoufi, 1999, Numerical methods for chemical engineers with matlab application, Prentice Hall PTR, New Jersey.

Conti, M. and C. Turchetti, 1994, Approximation of dynamical systems by continuous-time recurrent approximate identity neural networks, *Neural, Parallel & Scientific Computations* **2**, 299-322.

Duchon, J., 1976, Interpolation des fonctions de deux variables suivant le principle de la flexion des plaques minces, *RAIRO Analyse Numeriques* **10**, 5-12.

Fan, X.J., 1985, Viscosity, first normal-stress coefficient, and molecular stretching in dilute polymer solutions, *J. Non-Newt. Fluid Mech.* **17**, 125-144.

Feigl, K., M. Laso and H.C. Ottinger, 1995, CONNFFESSIT Approach for solving a two-dimensional viscoelastic fluid problem, *Macromolecules* **28**, 3261-3274.

Fixman, M., 1978a, Simulation of polymer dynamics. I. General theory, *J. Chem. Phys.* **69(4)**, 1527-1537.

Fixman, M., 1978b, Simulation of polymer dynamics. II. Relaxation rates and dynamic viscosity, *J. Chem. Phys.* **69(4)**, 1538-1545.

Franke, R., 1982, Scattered data interpolation: test of some methods, *Math. Comput.* **48**, 181-200.

Gardiner, C.W., 1990, Handbook of stochastic methods for physics, chemistry and the natural sciences, Springer-Verlag, Berlin.

Gihman, I.I. and A.V. Skorohod, 1974, The theory of stochastic processes III, Springer-Verlag, Berlin.

Hardy, R.L., 1971, Multiquadric equations for topography and other irregular surfaces, *J. Geophys. Res.* **176**, 1095-1915.

Haykin, S., 1999, Neural networks: A comprehensive foundation, Prentice Hall, New Jersey.

He, S., K. Reif and R. Unbehauen, 2000, Multilayer neural networks for solving a class of partial differential equations, *Neural Networks* **13**, 385-395.

Herrchen, M. and H.C. Ottinger, 1997, A Detailed comparison of various FENE dumbbell models, *J. Non-Newt. Fluid Mech.* **68**, 17-42.

Hulsen, M.A., A.P.G. van Heel and B.H.A.A. van den Brule, 1997, Simulation of viscoelastic flows using Brownian Configuration fields, *J. Non-Newt. Fluid Mech.* **70**, 79-101.

Kansa, E.J., 1990, Multiquadrics-A scattered data approximation scheme with applications to computational fluid dynamics-II: Solutions to Parabolic, Hyperbolic and Elliptic Partial Differential Equations, *Computers Math. Applic.* **19(8-9)**, 147-161.

Keunings, R., 1996, On the Peterlin approximation for finitely extensible dumbbells, *J. Non-Newt. Fluid Mech.* **68**, 85-100.

Kloeden, P.E., E. Platen and H. Schurz, 1997, Numerical solution of SDE through computer experiments, Springer, Berlin.

Kloeden, P.E. and E. Platen, 1997, Numerical solution of Stochastic Differential Equations, Springer, Berlin.

Laso, M. and H.C. Ottinger, 1993, Calculation of viscoelastic flow using molecular models: the CONNFFESSIT approach, *J Non-Newt. Fluid Mech.* **47**, 1-20.

Laso, M., M. Picasso and H.C. Ottinger, 1997, 2-D Time-dependent viscoelastic flow calculations using CONNFFESSIT, *AIChE Journal* **43(4)**, 877-892.

Laso, M., M. Picasso and H.C Ottinger, 1999, Calculation of flows with large elongation components: CONNFFESSIT calculation of the flow of a FENE fluid in a planar 10:1 contraction. In: Nguyen, T.Q. and Kausch, H.H., flexible polymer chains dynamics in elongational flow: theory and experiment, Chapter 6, 101-136, Springer, Berlin.

Mai-Duy, N. and T. Tran-Cong, 2001, Numerical solution of Navier-Stokes equations using multiquadric radial basis function networks, *Neural Networks* **14**, 185-199.

Mochimaru, Y., 1983, Unsteady-state development of plane Couette flow for viscoelastic fluids, *J. Non-Newt. Fluid Mech.* **12**, 135-152.

Onate, E., S. Idelsohn, O.C. Zienkiewicz and L. Taylor, 1996, A finit point method in computational mechanics. Applications to convective transport and fluid flow, *Int. J. Numer. Meth. Engng.* **39**, 3839-3866.

Orr, M.J.L., 1997, Matlab routines for subset selection and ridge regression in Linear Network, *http://www.cns.ed.ac.uk/~mjo.*

Orr, M.J.L., 1999, Regularisation in the selection of radial basis function centres, *http://www.cns.ed.ac.uk/~mjo.*

Ottinger, H.C., 1996, Stochastic processes in polymeric fluids: tools and examples for developing simulation algorithms, Springer, Berlin.

Ottinger, H.C., B.H.A.A. van den Brule and M.A. Hulsen, 1997, Brownian configuration fields and variance reduced CONNFFESSIT, *J. Non-Newt. Fluid Mech.* **70**, 255-261.

Park, J. and I.W. Sandberg, 1991, Universal approximation using radial basis function networks, *Neural Computation* **3**, 246-257.

Smith, G.D., 1978, Numerical solution partial differential equations: Finite Difference Methods, Clarendon, Oxford.

Tran-Canh, D. and T. Tran-Cong, 2002, BEM-NN computation of Generalised Newtonian Flows, *Eng. Anal. With Boundary Elements* **26**, 15-28.

Zerroukat, M., H. Power and C.S. Chen. 1998, A numerical method for heat transfer problems using collocation and radial basis functions, *Int. J. Numer. Meth. Engng.* **42**, 1263-1278.